analytical chemistry

Article

pubs.acs.org/ac

Electrochemical Reactions in Subfemtoliter-Droplets Studied with Plasmonics-Based Electrochemical Current Microscopy

Yixian Wang,[†] Xiaonan Shan,[†] Fengjuan Cui,[‡] Jinghong Li,[‡] Shaopeng Wang,[†] and Nongjian Tao*[,†]

[†]Center for Bioelectronics and Biosensors, Biodesign Institute, Arizona State University, Tempe, Arizona 85287-5706, United States

[‡]Department of Chemistry, Tsinghua University, Beijing 100084, China

Supporting Information

ABSTRACT: We report on a plasmonics-based electrochemical current imaging of redox reactions in aqueous droplets with diameters varying from a few hundred nanometers (tens of attoliter in volume) to a few micrometers. The imaging technique allows us to obtain cyclic voltammograms of multiple droplets on a gold electrode simultaneously and to examine the local redox reactions within a droplet. The results are supported by numerical simulations. The work demonstrates a new capability of studying electrochemistry in microdroplets, which offers an opportunity to understand electrochemical reactions within a small confined volume.

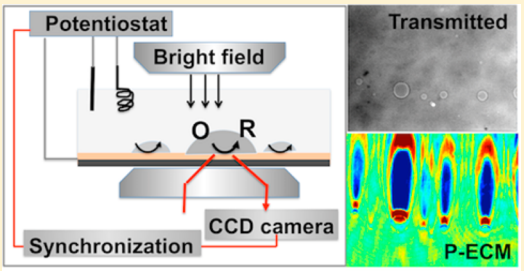

Studying electrochemical phenomena in a micro- and nanoscaled droplet offers an unique opportunity to understand electrochemistry at the smallest scales within a confined volume and with a small number of molecules.[1−6] Furthermore, as microdroplet-based single cell analysis (a cell in a droplet) becomes increasingly popular, a capability of studying electrochemistry in microdroplet could also provide electrochemical detection of electroactive species secreted from the cell confined in the droplet.[7,8]

Electrochemical reactions can be studied with microfabricated electrodes,[1−3,9−14] including scanning electrochemical microscopy (SECM),[15−18] and ion selective electrodes.[19,20] An important example is the detection of electroactive species, dopamine, in vesicles, with a microelectrode, which measures the transient electrochemical reaction current of dopamine as it is released from each vesicle diffuses to the microelectrode held at an appropriate potential[10,11] A recent work by Bard's group reported the detection of collision of a single attoliter droplet with an ultramicroelectrode.[21] These pioneering works provide an important foundation to the study of electrochemistry confined within a small volume. However, the microelectrode approach does not have imaging capability, making it difficult to detect multiple microdroplets simultaneously.[22−26] The use of an array of microelectrodes[27] allows the analysis of multiple droplets, but the fabrication of a high-density microelectrode array and electrical readout from each microelectrode in the array present a technical challenge. SECM offers imaging capability, but it requires mechanical scanning of a microelectrode, which limits its imaging speed.

Here we present a study of electrochemical reactions of single micro- and nanoscaled droplets with plasmonics-based electrochemical current microscopy (P-ECM). The principle of P-ECM is to image local concentration changes of electroactive species near an electrode surface as a function of potential and time with surface plasmon resonance (SPR). From the potential- and time-dependent SPR signals, local electrochemical current[28] and impedance[29] are imaged. Using P-ECM, we have imaged heterogeneous electrochemical reactions on an electrode, detected trace chemicals, and measured the electrocatalytic properties of single nanoparticles.[28−33] Different from the previous works, the present work aims to develop P-ECM capability to study micro- and nanoscaled droplets, in which the electrochemical reactions are confined within small volumes. Using P-ECM, we have obtained cyclic voltammograms of multiple droplets with diameters varying from a few micrometers down to a few hundred nanometers on a gold electrode, studied the size dependence, examined the local redox reactions within a droplet, and modeled the results in terms of the Nernst equation and the plasmonic response to concentration change.

EXPERIMENTAL SECTION

Chemicals. The following chemicals were used as received from Sigma: NaF, potassium ferrocyanide ($K_4Fe(CN)_6$) and potassium ferricyanide ($K_3Fe(CN)_6$). All the aqueous solutions were prepared from deionized water (Milli-Q, Millipore Corp.).

Hydrophobic ionic liquids (ILs), 1-butyl-3-methylimidazolium hexafluorophosphate ($[C_4mim][PF_6]$), and 1-butyl-3-methylimidazolium bis(trifluoromethylsulfonyl)imide ($[C_4mim][Tf_2N]$), were synthesized in Prof. Jinghong Li's lab at Tsinghua University. The physical properties of the ILs are described in the Supporting Information. Both ILs were presaturated with water before experiments by shaking the mixture with a vortex mixer (Scientific Industries) for a few

Received: July 26, 2014
Accepted: December 5, 2014
Published: December 5, 2014

hours to avoid the absorption of water droplets during experiments.

Instrumentation. The details of the P-ECM were described in a previous publication.[30] Briefly the setup was built on an inverted microscope (Olympus IX81) equipped with a high numerical aperture oil-emersion objective. P-polarized light from a 670 nm superluminescent diode (SLD) (Superlum, PILOT-4) was directed onto the gold film mounted on the objective for SPR excitation, and the reflected light was collected with the same objective and directed to a CCD camera for imaging. The gold films were prepared by coating 47 nm gold on glass microscope coverslips.[30] The potential of the gold film was controlled with respect to a Ag/AgCl wire quasi-reference electrode and a Pt wire counter electrode by a potentiostat. The CCD camera was synchronized with potential cycling.

Preparation of Samples. Two methods were used to form aqueous droplets on the gold film. The first one was to sonicate the mixture of IL and aqueous solution containing 0.4 M NaF, 25 mM $K_3Fe(CN)_6$, and $K_4Fe(CN)_6$ with a volume ratio of ~6:1 for 20 s until the mixture turns cloudy and then to inject the mixture into the sample cell. The average size of the droplets was controlled by the sonication time. The second method was to directly spray the aqueous droplets on to the gold film and immediately cover them with IL.

P-ECM Imaging of Ferricyanide and Ferrocyanide Redox Reaction. After mounting the prepared sample, the droplets were first imaged in the bright field mode using a white light illuminator from the top (see Figure 1B). The sample was

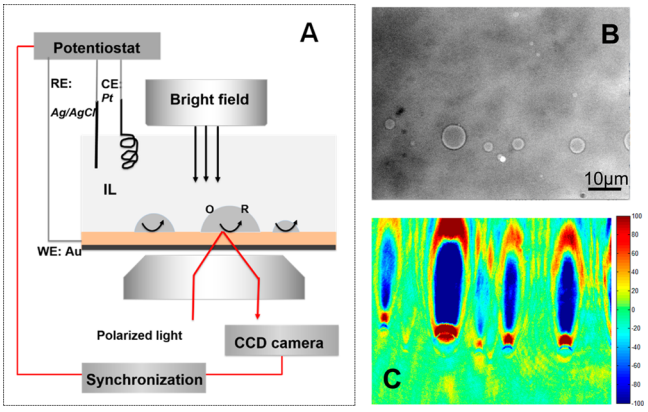

Figure 1. Schematic of the experimental setup (A), representative transmitted image (B), and P-ECM image (C) of a group of droplets. The scale bar in part C represents relative intensity.

then imaged with the P-ECM. Associated with each droplet is a long tail pointing in the direction of the surface plasmonic wave, which was due to the scattering of the waves by the droplets. A similar observation was discussed in a previous publication by us.[31] Note that the droplet and the tail regions showed opposite responses. After adjusting the exposure time of the CCD camera, P-ECM images were recorded while sweeping the potential. For each measurement, 16-bit P-ECM images were recorded at frame rates up to 106.6 fps.

Data Extraction and Processing. The raw P-ECM images were batch-converted to 16-bit tiff format files using a Matlab program. The average P-ECM intensity was calculated over the selected area for all images, using ImageJ software. The intensity changes were calibrated to the millidegree (mDeg) of SPR angle shift, θ, based on the calibration result from bulk solution using 1% ethanol as the standard. The first image was subtracted from every frame, and all the frames were smoothed by a 5 × 5 pixels averaging. Figure 1C shows an example of the P-ECM image after fast Fourier transform (FFT) on the time-domain.

COMSOL Simulations. Numerical simulations were carried out with the Electroanalysis model in COMSOL 4.4. A simulation report as well as equations for boundary conditions have been included in the Supporting Information.

RESULTS AND DISCUSSION

We studied droplets containing 25 mM redox couple ferrocyanide and ferricyanide and 0.5 M NaF as the supporting electrolyte in aqueous solution on a gold electrode (gold-coated glass slide), which are mounted on an inverted optical microscope for P-ECM imaging (Figure 1A). The droplets were prepared by spraying the solution onto the gold electrode and then covered with ionic liquid. The smallest stable droplet has a diameter of 620 nm, corresponding to a volume of 29 aL, as shown with the bright field optical image (Figure 1B). We have attempted to make smaller droplets but they are unstable due to absorption of water by the ionic liquid. The potential of the gold electrode was controlled with a potentiostat by inserting a Ag/AgCl reference and Pt wire counter electrodes into the ionic liquid. Redox reactions in the individual droplets were imaged with P-ECM (Figure 1C). The image shown was obtained first by subtracting each frame with the first frame, applying a 5 × 5 pixel binning filter, and then performing FFT for each pixel. Note that the SPR image of each droplet shows a long tail in the direction of the surface plasmonic wave (upward direction). This is because of the propagation length of surface plasmons.

P-ECM is based on the sensitive dependence of SPR on the local concentration of electroactive species near an electrode surface. In the case of micro- and nanoscaled droplets, diffusion of the electroactive species is not expected to be a rate limiting step in the electrochemical reactions, which is analogous to thin-layer eletrochemistry.[34] In fact, considering ferrocyanide ions with diffusion coefficient of 6.7×10^{-6} cm^2/s, diffusion length is 26 μm over a time scale of 1 s, which is much greater than the sizes of the droplets studied here. Another assumption is that all the species are confined within the droplets (with a height to radius ratio of 1:1.8, according to optical measurements of contact angles). This assumption was later demonstrated by no obvious decrease of peak current of droplets during several scans. On the basis of the above assumptions, the electrochemical reaction current is related to the SPR signal (e.g., resonance angle shift) and given by

$$i = -nbFV\frac{\mathrm{d}\theta(x, y)}{\mathrm{d}t} \quad (1)$$

where b is a constant that can be calibrated experimentally, F is the Faraday constant, V is the volume of the droplet, and θ is the resonance angle shift (see more detailed discussion in the Supporting Information). On the basis of eq 1, local electrochemical current vs time and potential can be readily obtained from the time and potential dependent SPR signals. The SPR signal expressed in eq 1 is the SPR angle shift, which is proportional to the image intensity change when the angle of incident light is parked within an appropriate range of angle.[28−33] Note that when the droplet size becomes

comparable to or smaller than the optical diffraction limit, optical distortion of the droplet image must be considered, which is not taken into account by eq 1 (see the discussion below). Note also that no significant changes in the shape of the droplets with the potential were observed within the potential window of study (see Figure S4 in the Supporting Information).

Calibration. As mentioned previously, the observed averaged SPR intensity is size-dependent for small droplets, due to finite spatial resolution of the optical imaging. This size-dependent effect is corrected with the following equation,

$$i = -nYFV\frac{dI}{dt} \quad (2)$$

where I is the SPR image intensity and Y is a calibration factor that depends on the droplet size. The calibration curve of Y is plotted in Figure 2, showing that Y is inversely proportional to the square of the droplet diameter. The calibration of those two sets of data result in similar calibration factors. Note that the calibration does not depend on ionic strength because the method detects the change in the optical signal associated with oxidation and reduction but not the absolute intensities.

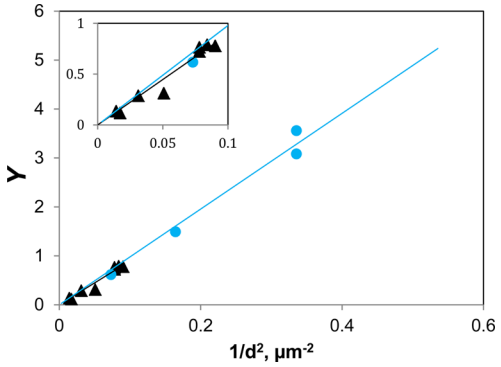

Figure 2. Calibration curve of droplets with different diameters. Different colors represent results obtained from three different samples. The fitting results are $Y = 10.4/d^2$ (blue) and $Y = 8.9/d^2$ (black).

Cyclic Voltammetry of Single Droplets. Using P-ECM, we obtained cyclic voltammograms (CVs) of the individual droplets. Figure 3 shows several snapshots of a CV for a 3.7 μm-diameter droplet at different potentials during one potential cycle. At −0.09 V, which is far away from the redox potential of ferricyanide, the P-ECM image contrast is negligible because no electrochemical reaction takes place. As the potential increases toward the redox potential, the contrast (current density) in the P-ECM image increase (red) as the oxidation of $K_4Fe(CN)_6$ takes place. The maximum positive contrast (positive current density) reaches a maximum at 0.05 V. As the potential continues to increase, the P-ECM contrast decreases and finally disappears at 0.21 V, corresponding to complete oxidation of $K_4Fe(CN)_6$ in the droplet. When the potential cycles back, the contrast is inverted (blue) which reflects the reduction of $K_3Fe(CN)_6$ and consequently a negative electrochemical current. When the potential cycles back to −0.09 V, the contrast disappears again.

Note that the time difference between the nearest images is about 0.05 s. The diffusion length over 0.05 s is about 3.4 μm, which is much larger than the height of the droplet (1 μm or even smaller); therefore, diffusion should not be a rate limiting step. This is further demonstrated by plotting the CVs and simulation results. By plotting the current vs potential, CVs of different droplets are obtained, which are shown in Figure 4A.

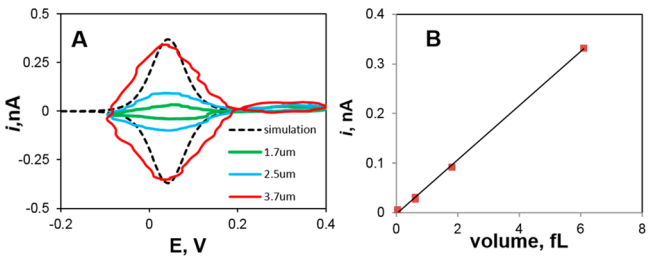

Figure 4. (A) CVs obtained from P-ECM for droplets with diameters of (red) 3.7 μm, (blue) 2.5 μm, and (green) 1.7 μm and where the dashed line is simulated CV. (B) Peak current (oxidation) vs droplet volume. The scanning rate was 1 V/s.

A simulated CV with COMSOL is also shown for comparison with the P-ECM results. Both the measured and simulated CVs show symmetric redox peaks, but the peaks in the experimental CVs are broader as the simulated CV. This broadening may be understood based on the following considerations. As ferrocyanide/ferricyanide oxidizes or reduces at the gold/water interface, counterions must transport across the water/IL interface in and out of the droplet in order to sustain a steady electrochemical current and maintain charge neutrality in the droplet.[35] If the ion transport across the water/IL interface is not fast enough, a substantial potential drop will occur at the

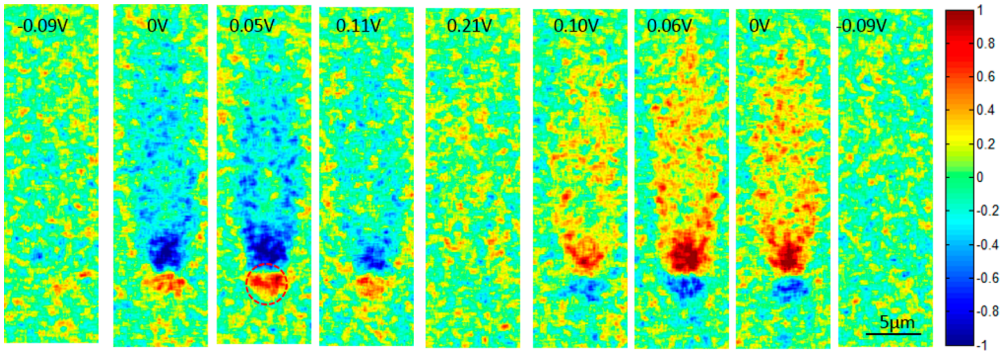

Figure 3. P-ECM images of a 3.7 μm-diameter droplet at different potentials during one potential cycle. The droplet contains 25 mM $K_3Fe(CN)_6$, 25 mM $K_4Fe(CN)_6$, and 0.5 M NaF. The colored bar represents the normalized current density scale. The red dashed circle in the third images marks the location of the droplet.

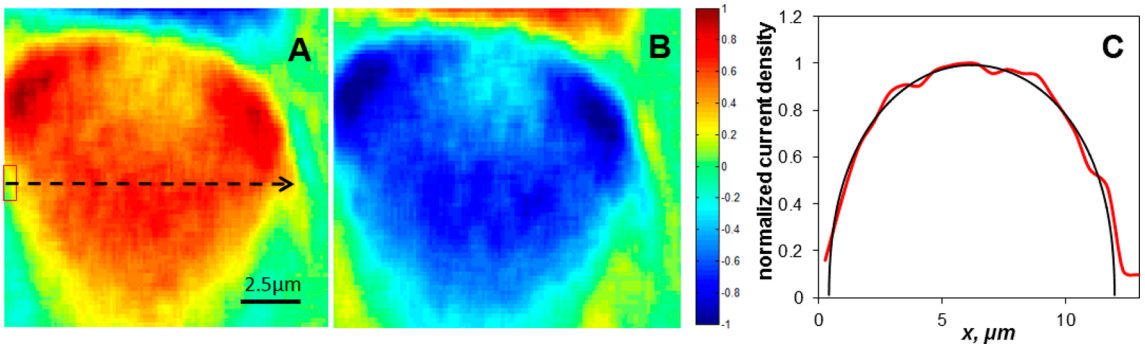

Figure 5. Distribution of local current density of a 13 μm-diameter droplet obtained with P-ECM at 0.05 V during the forward scan (A) and backward scan (B). (C) Current density distribution profiles along the dashed line shown in part A are obtained with P-ECM (red curve) and numerical simulation (black curve). Note that the current density plotted in part C was obtained by averaging over an area of 0.6 μm × 1.5 μm (red box in part A) along the dashed line.

interface, and charge neutrality may not be maintained, which could contribute to the observed broadening of CV. A broadened CV has been reported in a water/polymer membrane (as an organic phase)/Au system, where a potential drop associated with the oxidization and reduction of the polymer occurs at the water/polymer interface.[36]

Local Distribution within One Droplet. P-ECM also provides the local electrochemical reaction information within a droplet, a capability not available for the traditional microelectrode approach. Note that as we have discussed earlier, the P-ECM image of a small droplet is distorted by the propagation of surface plasmonic waves along the *y*-axis. However, the spatial resolution in the *x*-axis is only limited by optical diffraction, which is ~200 nm. Since the droplets are isotropic in the *x*−*y* plane, the P-ECM image in the *x*-axis reflects local distribution of electrochemical reaction current density. Figure 5A,B shows the P-ECM images at the peaks of oxidation and reduction, respectively. The current density distribution along the *x*-axis is shown in Figure 5C, which indicates a significant edge effect, i.e., smaller reaction current density near the edge of the droplet. This edge effect, as confirmed by numerical simulation (black curve in Figure 5C), is due to the depletion of redox species concentration gradient in the regions near the edge. The numerical simulation further indicates that local current density distribution within a droplet is highly dependent on the 3D geometry of the droplet (see Figure S2C in the Supporting Information).

Subfemtoliter-Droplets. In order to explore the detection limit, we have attempted to image the electrochemical reactions of smallest droplets possible. Although the formation of submicrometer-droplets was straightforward, droplets smaller than a few hundred nanometers were found to be unstable. This is because the solubility of water in $[C_4min][Tf_2N]$ is about 0.26 in mole fraction at room temperature based on the report by Freire et al.,[37] so small droplets become dissolved in the ionic liquid over time during the experiment. The smallest stable droplet we detected is about 0.62 μm in diameter, corresponding to ~29 aL in volume if assuming a height-to-radius ratio of 1:1.8. The transmitted image, P-ECM, and the converted CV are shown in Figure 6. An estimation of charges based on the CV is about 2.5×10^{-12} C. The 10 times error suggests that this droplet was about 10 times more concentrated than the original one, which can be explained by the absorption of water by IL decreasing the volume of the droplet. The background noise can also affect the detection of ultrasmall droplets, which can be improved by averaging over

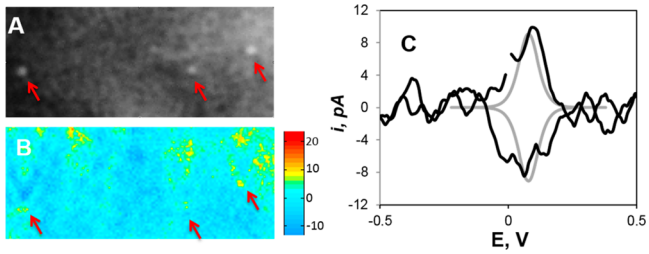

Figure 6. (A) Transmitted image and (B) P-ECM and (C) CV (obtained with P-ECM) for a 0.62 μm diameter droplet (black) and a simulated CV (gray).

multiple potential cycles. Note that for these submicrometer droplets, quantitative analysis is affected by the long-term stability of droplets. For this reason, we limit our analysis to freshly formed droplets with sizes that do not shrink during the measurement.

CONCLUSIONS

We have imaged local electrochemical reactions of aqueous droplets in an ionic liquid with P-ECM and obtained the CVs of single droplets of various sizes ranging from a few tens of micrometers to a few hundred nanometers. The size dependence is in good agreement with the theory and numerical simulation. The smallest droplet studied is ~29 aL in volume, and smaller droplets were not stable in the ionic liquid. The spatial resolution of P-ECM also allows analysis of the local distribution of the current density. The work demonstrates a new capability of studying electrochemistry in micro- and nanodroplets, which offers an opportunity to understand electrochemical reactions within a small confined volume. Compared to the previous microelectrode methods, P-ECM has imaging capability and can analyze multiple droplets simultaneously. However, quantitative comparison of P-ECM with the traditional electrochemical measurements requires calibration of the conversion factor from the plasmonic imaging intensity to an electrochemical current.

ASSOCIATED CONTENT

Supporting Information

Theory and COMSOL simulations. This material is available free of charge via the Internet at http://pubs.acs.org.

AUTHOR INFORMATION

Corresponding Author

*E-mail: njtao@asu.edu.

Notes

The authors declare no competing financial interest.

ACKNOWLEDGMENTS

The support of this work by the AFOSR MURI (Grant FA9550-14-1-0003) is gratefully acknowledged. We appreciate the professional suggestions from Prof. Shigeru Amemiya (University of Pittsburgh) and Prof. Michael Mirkin (Queens College, CUNY).

REFERENCES

(1) Li, T.; Su, L.; Hu, W.; Dong, H.; Li, Y.; Mao, L. *Anal. Chem.* **2010**, *82*, 1521−1526.
(2) Rossier, J. S.; Roberts, M. A.; Ferrigno, R.; Girault, H. H. *Anal. Chem.* **1999**, *71*, 4294−4299.
(3) Clark, R. A.; Ewing, A. G. *Anal. Chem.* **1998**, *70*, 1119−1125.
(4) Fan, F. -R. F.; Bard, A. J. *Science* **1995**, *267*, 871−874.
(5) Sun, P.; Mirkin, M. V. *J. Am. Chem. Soc.* **2008**, *130*, 8241−8250.
(6) Banks, C. E.; Davies, T. J.; Evans, R. G.; Hignett, G.; Wain, A. J.; Lawrence, N. S.; Wadhawan, J. D.; Marken, F.; Compton, R. G. *Phys. Chem. Chem. Phys.* **2003**, *5*, 4053−4069.
(7) He, M.; Edgar, J. S.; Jeffries, G. D. M.; Lorenz, R. M.; Shelby, J. P.; Chiu, D. T. *Anal. Chem.* **2005**, *77*, 1539−1544.
(8) Mazutis, L.; Gilbert, J.; Ung, W. L.; Weitz, D. A.; Griffiths, A. D.; Heyman, J. A. *Nat. Protoc.* **2013**, *8*, 870−891.
(9) Lin, Y.; Trouillon, R.; Safina, G.; Ewing, A. G. *Anal. Chem.* **2011**, *83*, 4369−4392.
(10) Wightman, R. M.; Jankowski, J. A.; Kennedy, R. T.; Kawagoe, K. T.; Schroeder, T. J.; Leszczyszyn, D. J.; Near, J. A.; Diliberto, E. J., Jr.; Viveros, O. H. *Proc. Natl. Acad. Sci. U.S.A.* **1991**, *88*, 10754−10758.
(11) Amatore, C.; Arbault, S.; Bouret, Y.; Guille, M.; Lemaître, F.; Verchier, Y. *Anal. Chem.* **2009**, *81*, 3087−3093.
(12) Amatore, C.; Arbault, S.; Bouton, C.; Drapier, J.-C.; Ghandour, H.; Koh, A. C. W. *ChemBioChem* **2008**, *9*, 1472−1480.
(13) Lin, Z.; Takahashi, Y.; Murata, T.; Takeda, M.; Ino, K.; Shiku, H.; Matsue, T. *Angew. Chem., Int. Ed.* **2009**, *48*, 2044−2046.
(14) Berberian, K.; Kisler, K.; Fang, Q.; Lindau, M. *Anal. Chem.* **2009**, *81*, 8734−8740.
(15) Zhao, X.; Diakowski, P. M.; Ding, Z. *Anal. Chem.* **2010**, *82*, 8371−8373.
(16) Chen, Z.; Xie, S.; Shen, L.; Du, Y.; He, S.; Li, Q.; Liang, Z.; Meng, X.; Li, B.; Xu, X.; Ma, H.; Huang, Y.; Shao, Y. *Analyst* **2008**, *133*, 1221−1228.
(17) Sun, P.; Laforge, F. O.; Abeyweera, T. P.; Rotenberg, S. A.; Carpino, J.; Mirkin, M. V. *Proc. Natl. Acad. Sci. U.S.A.* **2008**, *105*, 443−448.
(18) Hu, K.; Gao, Y.; Wang, Y.; Yu, Y.; Zhao, X.; Rotenberg, S. A.; Gökmeşe, E.; Mirkin, M. V.; Friedman, G.; Gogotsi, Y. *J. Solid State Electrochem.* **2013**, *17*, 2971−2977.
(19) Lew, R. R. *Plant Cell Physiol.* **2010**, *51*, 1889−1899.
(20) Messerli, M. A.; Collis, L. P.; Smith, P. J. S. *Biophys. J.* **2009**, *96*, 1597−1605.
(21) Kim, B.-K.; Boika, A.; Kim, J.; Dick, J. E.; Bard, A. J. *J. Am. Chem. Soc.* **2014**, *136*, 4849−4852.
(22) Marken, F.; Blythe, A. N.; Compton, R. G.; Bull, S. D.; Davies, S. G. *Chem. Commun.* **1999**, 1823−1824.
(23) Marken, F.; Blythe, A. N.; Wadhawan, J. D.; Compton, R. G.; Bull, S. D.; Aplin, R. T.; Davies, S. G. *J. Solid State Electrochem.* **2001**, *5*, 17−22.
(24) Davies, T. J.; Banks, C. E.; Nuthakki, B.; Rusling, J. F.; France, R. R.; Wadhawan, J. D.; Compton, R. G. *Green Chem.* **2002**, *4*, 570−577.
(25) Ulmeanu, S. H.; Lee, J.; Fermin, D. J.; Girault, H.H. J.; Shao, Y. *Electrochem. Commun.* **2001**, *3*, 219−223.
(26) Simm, A. O.; Chevallier, F. G.; Ordeig, O.; Javier del Campo, F.; Munoz, F. X.; Compton, R. G. *ChemPhysChem* **2006**, *7*, 2585−2592.
(27) Guerrette, J. P.; Percival, S. J.; Zhang, B. *J. Am. Chem. Soc.* **2013**, *135*, 855−861.
(28) Shan, X.; Patel, U.; Wang, S.; Iglesias, R.; Tao, N. *Science* **2010**, *327*, 1363−1366.
(29) Lu, J.; Wang, W.; Wang, S.; Shan, X.; Li, J.; Tao, N. *Anal. Chem.* **2011**, *84*, 327−333.
(30) Wang, S.; Huang, X.; Shan, X.; Foley, K. J.; Tao, N. *Anal. Chem.* **2010**, *82*, 935−941.
(31) Shan, X.; Díez-Pérez, I.; Wang, L.; Wiktor, P.; Gu, Y.; Zhang, L.; Wang, W.; Lu, J.; Wang, S.; Gong, Q.; Li, J.; Tao, N. *Nat. Nanotechnol.* **2012**, *7*, 668−672.
(32) Shan, X.; Wang, S.; Wang, W.; Tao, N. *Anal. Chem.* **2011**, *83*, 7394−7399.
(33) Huang, X.; Wang, S.; Shan, X.; Chang, X.; Tao, N. *J. Electroanal. Chem.* **2010**, *649*, 37−41.
(34) Bard, A. J.; Faulkner, L. R. *Electrochemical Methods: Fundamentals and Applications*, 2nd ed.; Wiley: New York, 2001.
(35) Scholz, F.; Komorsky-Lovrić, Š.; Lovrić, M. *Electrochem. Commun.* **2000**, *2*, 112−118.
(36) Kim, Y.; Amemiya, S. *Anal. Chem.* **2008**, *80*, 6056−6065.
(37) Freire, M. G.; Carvalho, P. J.; Gardas, R. L.; Marrucho, I. M.; Santos, L. M. N. B. F.; Coutinho, J.A. P. *J. Phys. Chem. B* **2008**, *112*, 1604−1610.